

Article

Synthesis of a Novel Adsorbent Based on Chitosan Magnetite Nanoparticles for the High Sorption of Cr (VI) Ions: A Study of Photocatalysis and Recovery on Tannery Effluents

Maram H. Zahra¹, Mohammed F. Hamza^{2,3,*} , Gehan El-Habibi⁴, Adel A.-H. Abdel-Rahman^{4,*}, Hamed I. Mira³, Yuezhou Wei^{2,5,*}, Saad H. Alotaibi⁶ , Hamada H. Amer⁶, Adel E.-S. Goda⁷ and Nora A. Hamad⁴

¹ Research Core for Interdisciplinary Sciences, Graduate School of Natural Science and Technology, Okayama University, Tsushima Naka, Kita, Okayama 700-8530, Japan; maram@okayama-u.ac.jp

² School of Nuclear Science and Technology, University of South China, Hengyang 421001, China

³ Nuclear Materials Authority, POB 530, El-Maadi, Cairo 11728, Egypt; hamedmira@yahoo.com

⁴ Chemistry Department, Faculty of Science, Menofia University, Shebin El-Kom 32511, Egypt; gehanelhabibi2255@yahoo.com (G.E.-H.); nhamad059@gmail.com (N.A.H.)

⁵ School of Nuclear Science and Engineering, Shanghai Jiao Tong University, Shanghai 200240, China

⁶ Department of Chemistry, Turabah University College, Taif University, Taif 21944, Saudi Arabia; s.alosaimi@tu.edu.sa (S.H.A.); h.amer@tu.edu.sa (H.H.A.)

⁷ Tanta Higher Institute of Engineering and Technology, Tanta 31739, Egypt; adelgoda1969@gmail.com

* Correspondence: m_fouda21@hotmail.com (M.F.H.); adelnassar63@yahoo.com (A.A.-H.A.-R.); yzwei@sjtu.edu.cn (Y.W.); Tel.: +20-111-668-1228 (M.F.H.); +20-122-167-8094 (A.A.-H.A.-R.); +86-771-322-4990 (Y.W.)



Citation: Zahra, M.H.; Hamza, M.F.; El-Habibi, G.; Abdel-Rahman, A.A.-H.; Mira, H.I.; Wei, Y.; Alotaibi, S.H.; Amer, H.H.; Goda, A.E.-S.; Hamad, N.A. Synthesis of a Novel Adsorbent Based on Chitosan Magnetite Nanoparticles for the High Sorption of Cr (VI) Ions: A Study of Photocatalysis and Recovery on Tannery Effluents. *Catalysts* **2022**, *12*, 678. <https://doi.org/10.3390/catal12070678>

Academic Editors: Chung-Hsin Wu and Ewa Kowalska

Received: 14 May 2022

Accepted: 20 June 2022

Published: 21 June 2022

Publisher's Note: MDPI stays neutral with regard to jurisdictional claims in published maps and institutional affiliations.



Copyright: © 2022 by the authors. Licensee MDPI, Basel, Switzerland. This article is an open access article distributed under the terms and conditions of the Creative Commons Attribution (CC BY) license (<https://creativecommons.org/licenses/by/4.0/>).

Abstract: This study aims to evaluate the functionalization of chitosan biopolymer with heterocyclic moieties of 2-thioxodihydropyrimidine-4,6(1H,5H)-dione used for enhancing the sorption of Cr ions from aqueous solution. A synthesized sorbent is a nanoscale particle (around 5–7 nm), which explains the fast kinetics of sorption. The sorbent is specified using elemental analysis (EA), FTIR, BET (nitrogen sorption desorption isotherms), TGA, and SEM-EDX analyses. Sorption properties are investigated using ultraviolet emission (UV) but also using visible light (L). In the sorption diagram, the high sorption uptake and fast kinetics observed using ultraviolet conditions are shown. This work is conducted by removing Cr ions from highly contaminated tannery effluents, which have a high concentration of Cr associated with other poisonous elements such as Cd(II) and Pb(II). Under the selected conditions, complete sorption is performed during the first 60 and 45 min with a capacity of 2.05 and 2.5 mmol Cr g⁻¹ for the crosslinked chitosan (without functionalization) in L and UV, respectively. This sorption is enhanced by functionalizing to 5.7 and 6.8 mmol Cr g⁻¹ at the L and UV, respectively, as well as improving the sorption kinetics to 35 and 30 min for both techniques, respectively. The PFORE, and (Langmuir and Sips equations) fit the kinetics and isotherms, respectively.

Keywords: treatment of industrial effluents; chromium removal; photocatalysis studying; uptake kinetics; pyrimidinedione derivative; eco-friendly adsorbent

1. Introduction

In recent decades, environmental pollution has been widely increased due to population expansion and terrible human activities [1–3]. Heavy metals, i.e., chromium, lead, cadmium, aluminum, and copper, are the main components of industrial effluents. These metals contaminate air, soil, and water without suitable treatment to expel them, causing critical environmental problems [4,5].

Chromium is a potentially hazardous species, which results mainly from human activities and some industries such as the leather, textile, and electroplating industries. It is a hard metal with an atomic number of 24 and a molecular mass of 51.1 g/mole. Chromium

species vary in chemical properties and toxicity. Among these, Cr(VI) is considered the most perilous as a natural contaminant toward the environment through various industrial activities. Due to the oxidizing effect of Cr(VI), it has mutations and is carcinogenic to living organisms. Therefore, chromium (mostly Cr(VI)) must be removed from the environment, soil, and water to conquer considerable problems because of its environmental accumulation. It is well known that the toxicity of Cr(VI) is reduced by converting it to Cr(III) [6,7].

Most recently, scientists developed novel and significant methods for chromium elimination. These methods are chiefly classified into physicochemical, electrochemical, and developed oxidation. Physicochemical techniques include chemical precipitation, adsorption, ion exchange, and membrane filtration. Electrochemical reduction, electrodialysis, and electrocoagulation are common examples of electrochemical technology. At the same time, nanotechnology and photocatalysis are advanced oxidation technologies that show remarkable efficiency in wastewater treatment [8,9].

Biopolymers (or natural polymers) are widely used in various toxic metal removals. Polysaccharides are considered the most used in natural polymers, which have broad environmental applications. Polysaccharides are organic biopolymers which have monosaccharides as ingredient units and are functionalized by NH_2 and OH groups. The vital importance of polysaccharides is due to their amino and hydroxyl functional groups (which open new facilities for modification), biocompatibility, and biodegradability. Owing to their special chemical structure, polysaccharides are used among various sorbents for Cr(VI) and most toxic environmental pollutant removals [10]. Additionally, they are characterized by their nontoxicity, cost-effectiveness, and eco-friendly nature [11]. Chitosan, gum, alginate, and celluloses are the most used biopolymers and effective sorbents for removing of pollutants [12,13].

Today, advanced oxidation technologies, especially photocatalysis, are included among the most important techniques used in the degradation of chemical pollutants [14]. Photocatalysis involves the generation of reactive species bearing oxygen on exposure of the photocatalyst to visible radiation or to ultraviolet emission [15]. These reactive species cause the degradation of several chemical pollutants [16]. Additionally, photocatalysis is recorded as an efficient method to oxidize/reduce various hazardous heavy metal ions such as Copper(II), Cadmium (II), Mercury (II), [17], etc. In recent years, photocatalytics have been vastly developed [18,19]. TiO_2 is considered the most broadly used due to its remarkable activity, low cost, and non-toxic behavior [20]. Photocatalytic reduction is cleaner than chemical reduction [21]. The most important reductive photocatalytics of sulfides/oxides, i.e., TiO_2 , WO_3 , ZnO , etc., are considerably reported. The photocatalytic reduction (of Cr(VI)) is mainly carried out by TiO_2 [22,23]. Heterogeneous photocatalysis (HP), can be performed under sunlight as a slightly novel technique for removing the Cr(VI) and some other pollutants. This may be considered a good way to develop green chemistry approaches [21,24,25].

Many studies have reported photocatalytic degradation by TiO_2 , ZnO , CeO_2 , Fe_2O_3 , WO_3 , and MgO [26–30]. Cheng et al. compared the photocatalytic reduction activity of oxide catalysts, TiO_2 , ZnO , WO_3 , and NaTaO_3 . The highest Cr (VI) removal ratios were observed with NaTaO_3 at pH 3 and in the presence of sodium sulfite, while ZnO and TiO_2 showed the best efficiency at neutral pH [31]. Photoreduction of the Cr(VI) using ZnO (under UV radiation) was represented by Chakrabarti et al. [23]. In a related study, Wu et al. showed the effect of reduction of Cr (VI) by the effect of CeO_2 nanotubes in the presence of oxalic acid and the reduction was performed at room temperature [32].

Based on the above properties, two sorbents were established on biopolymers and their sorption properties were investigated; magnetite chitosan (so-called MC: as reference material) and functionalized chitosan with pyrimidine derivative (herein as MC-TDPD) were investigated in this study. This was based on several stages; firstly, the synthesis of 2-thioxodihydropyrimidine-4,6(1H,5H)-dione: (so-called TDPD), which is characterized by FTIR and mass spectroscopy (for functional groups and M.Wt.). The second step is grafting of the TDPD on the prepared activated chitosan nanoparticles (this was previously designed through (i) the preparation of magnetite nanoparticles, (ii) the precipitation of chitosan nanoparticles, (iii) enhancing stability through crosslinking using epichlorohydrin (EPI),

and finally, (iv) the synthesis of the activated chitosan nanoparticles through treatment with an extra amount of EPI in ethanolic medium to produce a free methylene chloride group for the substitution reaction for the next step). The last step of the synthesis is grafting the prepared TDPD on the designed spacer arm chitosan particles. The final product was characterized by elemental analysis (EA), FTIR, BET, TGA, and SEM-EDX analyses. sorption was achieved toward chromate ions (firstly from synthetic solution) by investigating the pH effect, uptake kinetics, sorption isotherms, reuse (regeneration), and finally, the application toward the real solution of tannery effluents in the Egyptian tannery unit, that highly contaminated by chromate and associated with other heavy metals such as Cd, Pb, and Co. The sorbent showed high affinity for the removal of chromate ions with a high percentage that reached higher than 99% for sorbent dose (SD) 25–30 gL⁻¹.

2. Results

2.1. Sorbent Characterization

2.1.1. FTIR Analysis

Chemical modification was verified by FTIR spectroscopy for the pristine thiourea, synthesized 2-thioxodihydropyrimidine-4,6(1H,5H)-dione (TDPD), after grafting of the TDPD on chitosan particles (MCH) to yield (MC-TDPD), as well as for the sorbent after Cr(VI) sorption and after five cycles of sorption desorption.

The thiourea showed several identical peaks related mainly to NH and C=S, which appeared at 3375, 3291, and 3170 cm⁻¹ [33], and a broad band at 2673 cm⁻¹ for SH str. of thiol groups after tautomerization with amine moiety [34]. The peak at 1611 cm⁻¹ is related to the C=N str. (yields from the tautomerization) overlapped with N-H bend [33,35]. A series of peaks appeared in the fingerprint region, which appeared at 727 and 627 cm⁻¹ for NH₂ + CO wag. (out-of-phase) [36] and N-C-N in-plane (bend) overlapped with Fe-O [37–39]. These peaks were shifted/changed in intensity and new peaks appeared related to the modification processes. The most noticed change occurred through the decrease of the intensity of NH stretching for TDPD with two pikes at 3584 and 3392 cm⁻¹, while increasing the broadness as grafting successfully occurred (appeared at 3443 cm⁻¹ for the MC-TDPD). A new peak appeared at 3095 cm⁻¹ for the C-H aromatic of the heterocyclic moiety and disappeared by increasing the broadness of OH and NH in the MC-TDPD. As cyclization was performed, the new peaks at 1705 cm⁻¹ and (1626 and 1499 cm⁻¹) for the C=O of aromatic stretching and that for C=O, C=N str., and N-H bending, respectively [40], and peaks at 1155 cm⁻¹ for TDPD and 1097 and 1060 cm⁻¹ for the MC-TDPD, were related to the hydrocarbon moieties of the N-C str., NH₂ (rock.), C-O str bridge oxygen, and C-O-C str. (asymm) [41], while new bands at 923 and 854 cm⁻¹ for the TDPD and MC-TDPD, respectively, were related to the aromatic C-H bend for the heterocyclic moiety (in-plane). As Cr(VI) sorbed, most of these peaks were shifted and decreased in their intensities, especially for NH, C=O, OH, C=S, and SH (with expected tautomerization) [36,40,42,43], while after desorption for the five cycles, these bands restored as in the original sorbent before loading with metal ions, as shown in Figure S1. The specification of the most important bands is identified in Table 1.

Table 1. FTIR characterization of thiourea, TDPD, and MC-TDPD, after sorption and after five cycles of sorption desorption.

Assignment	Thiourea	TDPD	MC-TDPD	MC-TDPD+Cr	Sorbent after 5th Cycles	Ref.
N-H and OH str.	3375, 3291, 3170	3584, 3392	3443	3423	3398	[44,45]
C-H (aromatic str.)		3095				[46,47]
C-H (aliphatic str.)	2915, 2850	2867	2912, 2816	2920, 2847	2918, 2872	[48]
S-H str. of thiol group	2673	2583	2583		overlapped	[48]
Multiple bonded C-O			2046		2056	[48]
C=C aromatic str.		1705				[48]

Table 1. Cont.

Assignment	Thiourea	TDPD	MC-TDPD	MC-TDPD+Cr	Sorbent after 5th Cycles	Ref.
C=O, C=N str. and N-H bend.	1611	1659, 1554	1626, 1499	1633	1628	[46]
C-N str., C-H bond, and C-C str.	1467, 1410	1422	1410		1451	[46]
Arom. (secondary amine)		1338	1363	1380	1370	[48]
Tert. amine		1271	1303		1314	[48]
OH bend (in-plane) and C-O str.,		1243	1214		1235	[49,50]
N-C str. and NH ₂ (rock.)		1155		1088	1130	[44,49,51]
C-O str bridge oxygen and C-O-C str. (asymm)	1078		1097, 1060		1056	[46]
NH ₂ rock.			1015		1025	[44]
Aromatic C-H bend (in-plane)		923	854		899	[46,47]
NH ₂ + CO wag. (out-of-phase)	727	800				[44,48]
N-C-N in-plane (bend), and Fe-O	627	599	632	580	627	[52,53]
O-H out-of-plane (bend.)		541	541		575	[48]
C-S str.	485	453				[54,55]
Polysulfide str.	447	448	420		443	[48]

TME: tautomerization effect.

2.1.2. Thermogravimetric Analysis

The thermal decomposition of the functionalized sorbent appears in Figure S2. It shows three decomposition profiles, the first stage is related to water loss, which appeared at 270.8 °C (about 12.09%), and the second loss profile is related to the depolymerization of the polymer backbone, degradation of the amine groups, and carbonyl/thiocarbonyl functional groups. This step corresponds to ~23.1%, in the range of 270.8 to 375.5 °C. The final loss was recorded for the char formation, which was in the range of 375.5 to 496.7 °C. The total loss of this material (MC-TDPD) was close to 57.038%, which was a little higher than the theoretical calculation (the resumed materials are related to Fe₃O₄ (around 30%), and the rest ratio is related to carbon). The DrTG has five loss stages represented at 57.56 °C, 290.6 °C, and 399.9 °C, and there are also another two peaks with low-intensity shoulders at 595.6 °C and 761.2 °C, as shown in Figure S2.

2.1.3. Morphology and Textural Properties

From the SEM photos of magnetite chitosan nanoparticles (MCH) and MC-TDPD from Figure 1a, the sorbents appeared with an average size of around 5–10 µm with irregular shapes, while the TEM Figure 1b confirms the presence of magnetite as a nanoscale size embedment into the polymer hydrocarbon; it appears as dense dark spherical spots with uniform shape. The dark condenses in some parts of the matrix are due to the agglomeration of the magnetite, while the size ranges between 2–5 nm.

The S_{BET} (specific surface area) and V_p (porous volume) of the sorbents were measured through nitrogen sorption desorption isotherms with values of 22.9 m² g⁻¹ and 6.8 cm³ STP g⁻¹, respectively, (for MCH). These values were affected by the grafting procedure, which reached around 24.1 m² g⁻¹ and 8.2 cm³ STP g⁻¹, respectively, (for MC-TDPD).

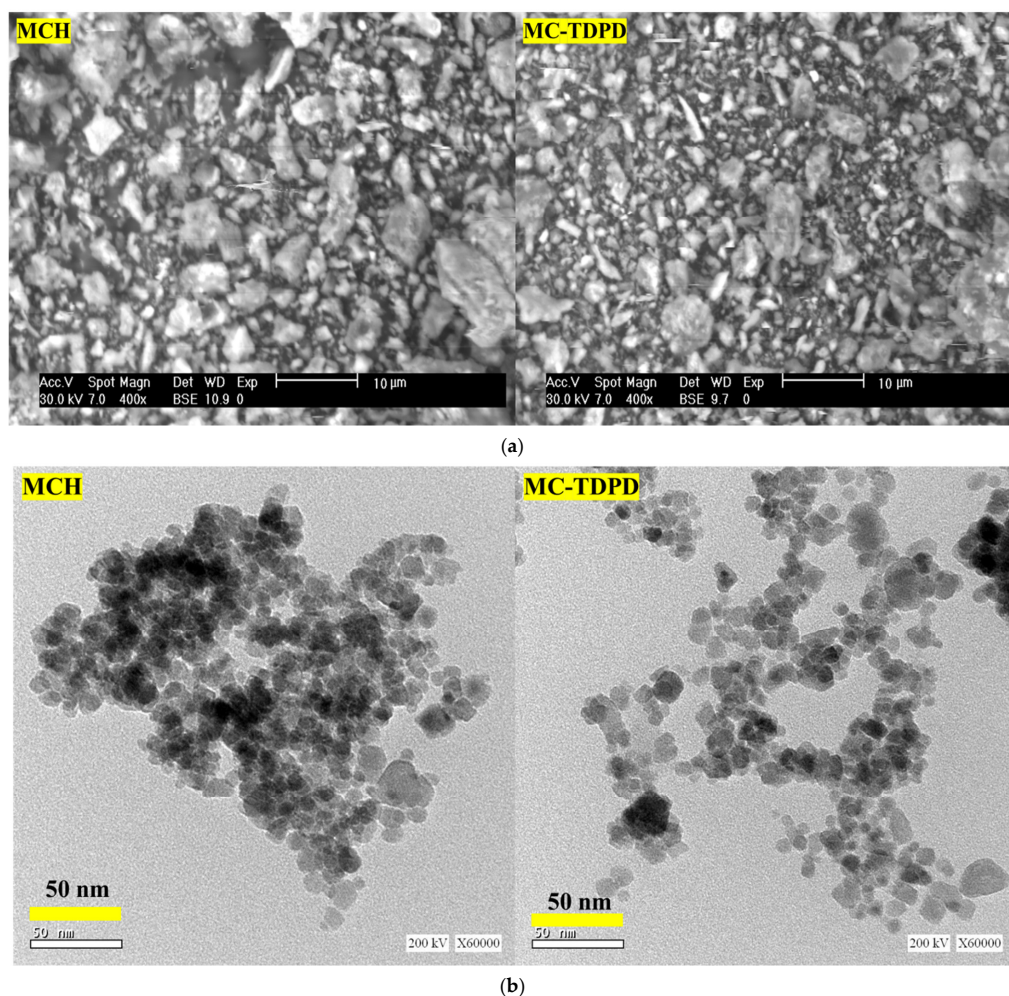


Figure 1. (a) SEM analysis of MCH and MC-TDPD sorbents. (b) TEM photos of MCH and MC-TDPD sorbents.

2.1.4. Elemental Analysis

From the elemental analysis data in Table S1, an increase in the percentage of N and O was noticed in the MC-TDPD composite (5.63 and 32.96%, respectively) compared to the original crosslinked chitosan particles, which are known as the reference material (MCH; 3.98 and 27.14%, respectively). Sulfur also appeared with a percentage of 1.11% in the MC-TDPD, verifying the successful grafting of the TDPD substrates.

2.1.5. Surface Charge Analysis- pH_{PZC}

The synthesis procedure shows the association of heterocyclic moieties in the chitosan surface with the change of the amine environment (used in the grafting). This leads to a change in the acid–base characterization. Figure S3 show the results profile of the MCH and MC-TDPD composites using the pH-drift method. The pH_{PZC} is shifted from 6.059 to 5.66 for MCH and MC-TDPD, respectively. This concludes that the sorbent becomes completely deprotonated after these values, and the electron pairs are available for the chelation type, in which the functional groups bear negative charge.

2.2. Sorption Properties from Synthetic Solutions

2.2.1. pH Effect

The pH has a direct effect on the reactive groups' dissociation found at the surface of the sorbent but also affects the metal speciation. Figure S4 show the chromium species distribution under the selected experimental conditions. The mainly anionic species such

as HCrO_4^- , $\text{CrO}_3\text{SO}_4^{2-}$, and $\text{Cr}_2\text{O}_7^{2-}$. Are found at acidic pH values. At pH higher than 5, the CrO_4^{2-} appeared and predominated at pH above 6.46.

Figure 2a compare the average of the sorption capacity (for the triplicate experiments) with the standard deviation as a function of pH equilibrium (pH_{eq}) for the functionalized and non-functionalized chitosan in visible light and UV effects. From the low values of standard deviation, a successive reproducibility of the sorbent was found. The increase in sorption performances as the functionalization was performed and compared it with the non-functionalized composite, showing the valorization of the grafting procedure. On the other hand, the increase in the loading performances by the effect of UV on sorption properties compared with the uses of visible light was shown. The sorption capacity was increased from $0.9 \text{ mmol Cr g}^{-1}$ to $3.34 \text{ mmol Cr g}^{-1}$ for MCH and MC-TDPD, respectively. This sorption occurred at pH 4 and 3, respectively, for normal visible light, in which these data were affected by the effect of light uses that increased by UV to 1.07 and $3.74 \text{ mmol Cr g}^{-1}$, respectively. This method can be used as a catalyst to recover Cr ions from acidic solutions. Vieira et al. [56] reported an efficient reduction of the chromate ions on different membrane types of chitosan.

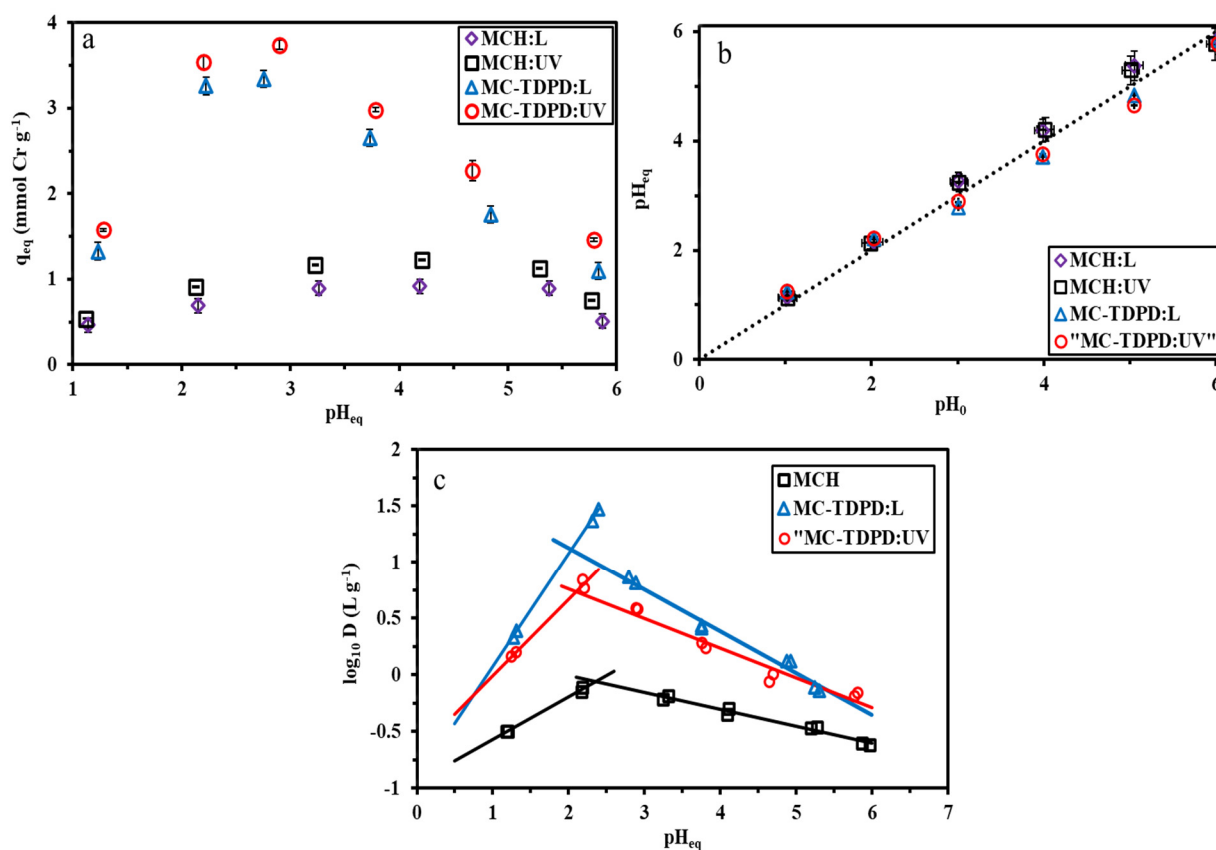


Figure 2. Studying the pH effect on sorption performances (a), pH variation during sorption (b), and the plotting results of $\log_{10} D$ units (c) as a function of pH_{eq} for MCH and MC-TDPD.

Figure 2b show the pH variation, which reports a slightly increased equilibrium pH for MCH (less than 0.4 pH unit), while the functionalized chitosan is slightly decreased (around 0.3 pH units). Figure 2c report the plot of $\log_{10} D$ units as a function of $\text{pH}_{\text{Equation}}$. The curves are divided into two sections. The slopes were determined and the curves (acidic medium) were +0.35, +0.62, and +0.61 for MCH, MC-TDPD:L, and MC-TDPD:UV, respectively. The slopes were also recorded for the right side to be -0.13, -0.35, and -0.29, respectively, indicating the use of ion exchange in the sorption procedure during Cr adsorption.

2.2.2. Uptake Kinetics

Figure 3 show the uptake kinetics of both sorbents before and after functionalization in light and UV. It reports that the equilibrium was reached after 60 and 45 min for the MCH in the light and UV, respectively, while improving the kinetic properties for the functionalized sorbent in terms of kinetic behavior, which reached 35 and 30 min at light and UV, respectively. The sorbents were found as nanoparticles with an expected thin layer of organic on the magnetite particles. This limits the intraparticle diffusion (resistance to diffusion) for metal ions in the sorbent pores (poorly porous), and this is the main reason for fast kinetics. The kinetic models were reported in Table S2, while Table 2 show the equilibrium parameters and capacities (calculated compared with experimental values). Regardless of the equilibrium sorption capacities (experimental vs. calculated) and the AIC parameters, this confirms the most fitted model is PFORE (pseudo-first-order rate equation) compared to PSORE (pseudo-second-order rate equation) and RIDE (resistance to intraparticle diffusion).

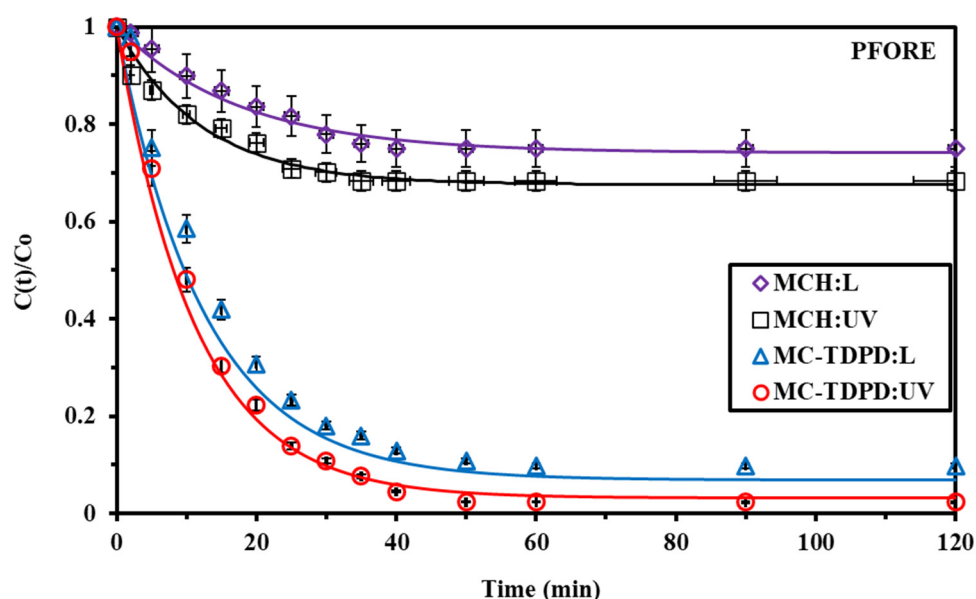


Figure 3. Cr(VI) uptake kinetics using MCH, MC-TDPD in light and UV conditions. Modeling with the PFORE.

Table 2. Parameters of the PFORE, PSORE, and RIDE for Cr(VI) uptake kinetics for the three experiments.

Model	Parameter	Visible Light			UV Emission		
		1	2	3	1	2	3
Exp.	q_{eq} (mmol Cr g ⁻¹)	0.97	0.99	0.96	1.27	1.32	1.38
PFORE	$q_{eq,1}$ (mmol Cr g ⁻¹)	1.01	0.13	0.97	1.29	1.3	1.35
	$k_1 \times 10^2$ (min ⁻¹)	4.98	5.02	5.12	6.33	6.49	6.51
	R ²	0.997	0.978	0.981	0.983	0.992	0.988
	AIC	-74.5	-91.6	-86.5	-123.5	-97.3	-105.7
PSORE	$q_{eq,2}$ (mmol Cr g ⁻¹)	1.39	1.27	1.32	1.01	0.98	0.99
	$k_2 \times 10^2$ (L mmol ⁻¹ min ⁻¹)	2.87	3.14	3.08	1.88	1.76	1.58
	R ²	0.863	0.779	0.698	0.913	0.896	0.905
RIDE	$D_e \times 10^8$ (m ² min ⁻¹)	9.97	8.85	8.49	3.76	4.01	4.13
	R ²	0.925	0.928	0.946	0.933	0.951	0.958
	AIC	-42.1	-38.3	-36.5	-45.4	-49.8	-55.3

Figure 3 show the average sorption kinetics for the three repeated experiments for MCH and MC-TDPD under light and UV emission, while Figure S5 show the unfit models of PSORE and RIDE. An interesting interpretation of the uptake kinetics was reported by Hubbe [57] and Simonin [58]. The type of mechanism (physical vs. chemical sorption) should depend on the experimental condition which controls this type. As expected from the study, Cr removal greatly increased by using MC-TDPD compared to MCH as well as in the UV condition over that of the light condition.

2.2.3. Sorption Isotherms

This method is used in the evaluation of the sorbent affinity toward the metal ion as well as maximum sorption capacity. The parameters of the models for the sorption isotherms are arranged in Table S3. The functionalized sorbent shows a steep sorption capacity before a tendency to plateau at saturation. The data for the functionalized sorbent and the crosslinked chitosan are represented in Figure 4 for the average of the three repeated experiments with the standard deviation, which is low to verify the reproducibility properties. The sorption properties were compared with the reference material (MCH). The sorption enhancement was determined through the increase of the maximum sorption capacity and initial slope according to MC-TDPD:UV > MC-TDPD:L >>> MCH:UV > MCH:L, which follow the same order of magnitude of the q_m values as shown in Tables 3 and 4. Three models were used for this evaluation to fit the sorption isotherms (Langmuir, Freundlich, and Sips equations, as reported in Table S3).

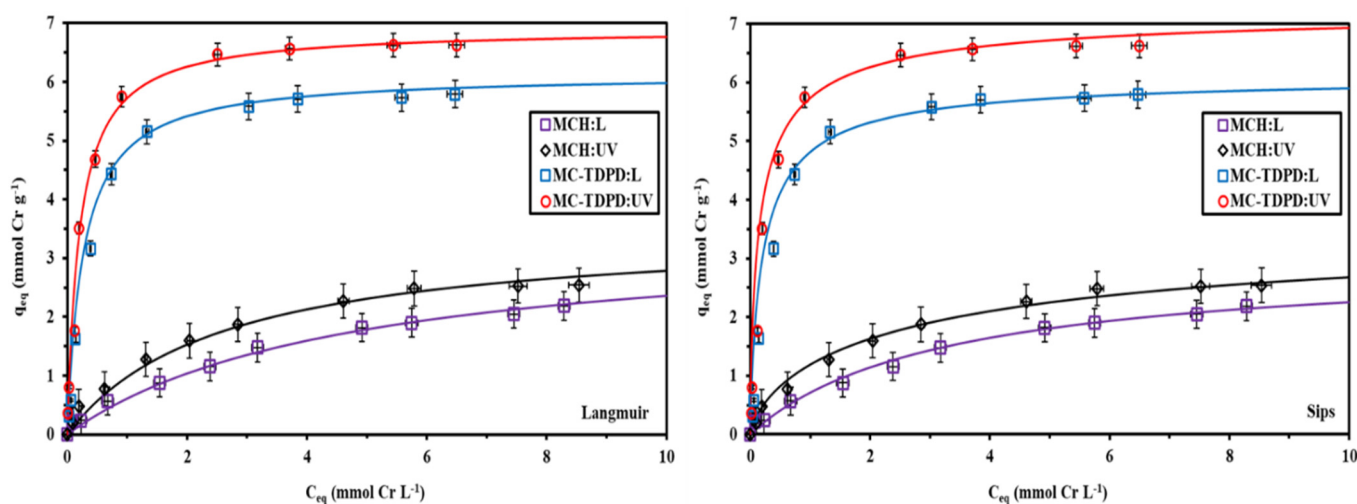


Figure 4. Cr(VI) sorption isotherms using MCH and MC-TDPD in light and UV conditions. Modeling with the Langmuir and Sips equations.

The Langmuir and Sips equations were fitted to the sorption isotherms, comparing them to the Freundlich equation, as shown in Figure S6. It is noteworthy that the Langmuir equation model corresponds to the mechanistic model (the sorption performed through monolayer, with homogeneous energies distribution). In other words, it is performed without interaction between sorbent molecules. The Freundlich equation is considered a mathematical equation with heterogeneous sorption, which has a hypothesis about the possible interactions of sorbed molecules. The third model of the Sips equation is a combination between the Freundlich and Langmuir equations, with a third parameter (n) that makes it easier to fit the experimental data.

Table 5 show the sorption performances of different sorbents found in the literature with a comparison of some properties that investigate the sorption advantages as the time of total sorption, b_L , pH of optimum sorption, and the maximum sorption capacity (calculated vs. experimental sorption). From these data, it was shown that sorbent is a promising tool for the recovery of Cr from polymetallic solution.

Table 3. Modeling Cr(VI) sorption isotherms. For MCH sorbent under visible light and UV emission.

Model	Parameter		Visible Light			UV Emission		
			1	2	3	1	2	3
Experimental	$q_{m,exp.}$	mmol Cr g ⁻¹	1.97	2.01	2.06	2.61	2.58	2.51
Langmuir	$q_{m,L}$	mmol Cr g ⁻¹	2.01	1.97	2.18	2.70	2.61	2.53
	b_L	L mmol ⁻¹	0.967	0.874	1.86	3.654	3.85	2.983
	R ²	-	0.9846	0.9931	0.9843	0.9846	0.9913	0.9892
	AIC	-	-65.88	-84.38	-79.41	-95.3	-103.2	-89.67
Freundlich	k_F	mmol ^{1-1/n} g ⁻¹ L ^{1/n}	0.896	0.906	1.196	3.29	4.315	2.188
	n_F	-	1.86	2.185	1.893	3.28	4.322	3.275
	R ²	-	0.8954	0.7998	0.9151	0.7837	0.8217	0.8573
	AIC	-	-25.53	-31.91	-22.84	-19.64	-31.18	-28.77
Sips	$q_{m,S}$	mmol Cr g ⁻¹	1.23	1.98	2.16	2.69	2.63	2.55
	b_S	L mmol ⁻¹	0.765	0.8876	0.8965	1.274	1.11	1.24
	n_S	-	1.32	1.48	1.44	2.464	2.28	2.314
	R ²	-	0.9786	0.9946	0.9895	0.9925	0.9936	0.9867
	AIC	-	-123.63	-163.94	-147.38	-115.38	-132.18	-128.48

Table 4. Modeling Cr(VI) sorption isotherms of MC-TDPD under visible light and UV emission.

Model	Parameter		Visible Light			UV Emission		
			1	2	3	1	2	3
Experimental	$q_{m,exp.}$	mmol Cr g ⁻¹	5.76	5.69	5.72	6.59	6.63	6.61
Langmuir	$q_{m,L}$	mmol Cr g ⁻¹	5.81	5.61	5.69	6.62	6.70	6.66
	b_L	L mmol ⁻¹	2.18	2.97	3.22	5.49	6.95	4.99
	R ²	-	0.9937	0.9894	0.9784	0.9936	0.9917	0.9936
	AIC	-	-127.27	-132.28	-119.38	-143.29	-128.28	-174.83
Freundlich	k_F	mmol ^{1-1/n} g ⁻¹ L ^{1/n}	2.18	1.86	1.968	2.886	3.054	3.18
	n_F	-	2.18	3.53	3.86	4.939	5.043	5.281
	R ²	-	0.7968	0.8164	0.8226	0.8362	0.8265	0.8736
	AIC	-	-36.182	-41.37	-37.84	-38.26	-18.47	-25.56
Sips	$q_{m,S}$	mmol Cr g ⁻¹	5.697	5.721	5.785	6.62	6.61	5.59
	b_S	L mmol ⁻¹	1.12	1.434	1.327	2.18	2.41	3.05
	n_S	-	2.17	2.65	2.19	3.023	3.26	3.426
	R ²	-	0.9956	0.9895	0.9942	0.9938	0.9967	0.9895
	AIC	-	-97.68	-117.68	-118.48	-135.4	-143.19	-144.3

Units: q: mmol g⁻¹, b_L: L mmol⁻¹.**Table 5.** Comparison of sorption performance for MCH and MC-TDPD with conventional sorbents.

Sorbent	pH	t _{eq} (min)	q _{m,exp}	q _{m,L}	b _L	Ref.
QPEI-SiO ₂	7	70	2.75	2.92	n.r.	[59]
Peat sorbent	4.5	1200	n.r.	0.154	0.208	[60]
<i>Auricularia a.</i> with CTAB dreg biochar	2	120	n.r.	0.479	7.80	[61]
Magnesium/zinc/ferrite	7	1440	0.586	0.65	25.0	[62]
pVP/DVB gel (Quaternized) resin	3–4	120	n.r.	2.75	1.15	[63]
Bacteria-PVA-alginate	6	1440	n.r.	0.46	29.0	[64]
Funct. Vinylpyridine-DVB sorbent	3–5	120	n.r.	1.44	0.743	[65]
Ionic liquid impregnated (MOF)	2	300	n.r.	5.49	6.72	[66]
Biogenic Fe-compounds	4	120	n.r.	0.14	2.72	[67]
NaY-Zeolite of rice husk ash	3	300	0.032	0.031	0.37	[68]
Amidoxime-funct. (pVBC)	n.r.	60	2.67	2.83	0.015	[69]
Quaternized functional cellulose	10	15	0.073	0.75	6.76	[70]

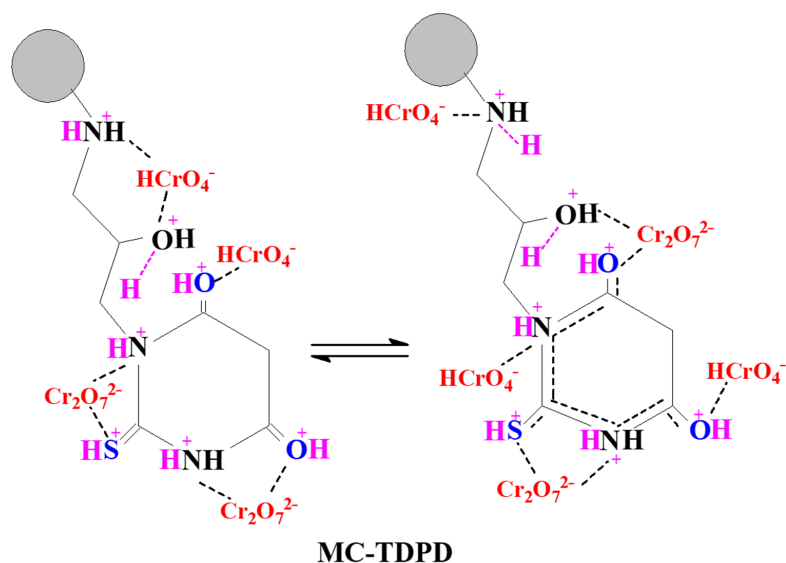
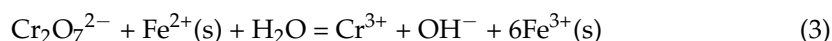
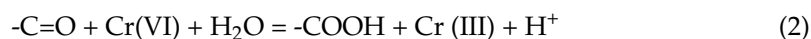
Table 5. Cont.

Sorbent	pH	t _{eq} (min)	q _{m,exp}	q _{m,L}	b _L	Ref.
Acid-activ. banana peel	4	120	0.288	0.293	2.08	[71]
ATA@MC sorbent	2	60	5.43	5.44	2.61	[72]
Fe-Fe ₂ O ₃ -PHCP nanochains	2	30	4.40	5.45	11.2	[73]
<i>Ulva-compressa</i> (L.) seaweed	2	120	0.418	0.417	46.3	[74]
Methylene Blue-Urea-Alginate	5.4	180	1.50	2.01	4.46	[75]
CTAB-carbonized coal	2	120	1.15	1.51	2.03	[76]
MCH:L	4	55	2.013	2.053	1.234	This work
MCH:UV	4	55	2.566	2.613	3.496	This work
MC-TDPD:L	3	30	5.723	5.7033	2.79	This work
MC-TDPD:UV	3	25	6.61	6.66	5.81	This work

n.r.: not reported.

2.2.4. Binding Mechanism

From the data collected from the FTIR, pHpzc, chromate speciation diagram, and pH studies, it was concluded that the sorption of chromate is performed at acidic pH with complete protonation of the functional groups (see the pHpzc studies). The protonated functional groups were electrostatic attraction with the negatively charged chromate ions. The FTIR shows the decreasing intensity of OH and NH bands as well as new groups for N⁺, which indicates the use of these groups in the binding mechanism and efficient protonation of OH and NH functional groups. Scheme 1 shows the expected binding mechanism of the chromate from the acidic medium during treatment with MC-TDPD sorbent, which indicates the exchange with hydroxyl groups, expected reduction of Cr(VI) by the effect of organic to Cr(III), and chelation reaction with amine groups. This is parallel with the results obtained by Cui et al. [77], who also suggest the reduction mechanism as follows from Equations (1)–(4).



Scheme 1. Expected binding mechanism of chromate ions with MC-TDPD sorbent at acidic pH medium.

2.2.5. Metal Desorption and Sorbent Recycling

Metal ion desorption and the sorbent recycling processes are important parameters in the evaluation of the sorption process. Sorption was performed in an acidic medium for the MC-TDPD and slightly acidic for the MCH sorbent (pH₀ 3 and 4, respectively). The acidic solution has an opposite effect on the sorption of chromate ions in the loaded sorbent, using the acidic solution in terms of the desorption of the sorbed metal ions. Recycling was performed for both sorbents in the light and ultraviolet emissions. From previous work, there is a very limited degradation of the magnetite core (around 1.5%) [39,78,79] after five cycles using a 0.5 M HCl solution; herein, we use 0.2 M HCl, so the loss is negligible. Table 6 report the five cycles of sorption desorption on the sorbent performances. It was found to have a limit loss in the efficiency of 3.1, 2.9, 2.78, and 2.55 for MCH:L, MCH:UV, MC-TDPD:L, and MC-TDPD:UV, respectively. This indicates the high stability of the sorbent. This appeared in the FTIR analysis, which indicates the restoration of the function groups after being used in the binding to chromate.

Table 6. Sorption/desorption recycling of MCH:L, MCH:UV, MC-TDPD:L, and MC-TDPD sorbents.

Cycles	MCH:L				MCH:UV			
	Removal (%)	S.D. (R.%)	Desorption (%)	S.D. (De%)	Removal (%)	S.D. (R.%)	Desorption (%)	S.D. (De%)
1	24.184	0.212	100	0.198	26.59	0.483	99.76	0.844
2	23.535	0.98	99.31	0.729	26.02	0.674	99.94	0.784
3	22.694	0.937	100	0.607	25.89	0.774	99.65	0.654
4	22.513	0.894	100	0.485	25.473	0.904	99.93	0.894
5	21.697	1.1275	99.923	0.968	24.998	0.985	99.91	0.784
Cycles	MC-TDPD:L				MC-TDPD:UV			
	Removal (%)	S.D. (R.%)	Desorption (%)	S.D. (De%)	Removal (%)	S.D. (R.%)	Desorption (%)	S.D. (De%)
1	78.187	0.8538	99.142	0.952	84.37	0.7463	99.97	0.746
2	77.491	0.548	99.649	0.496	83.87	0.644	99.856	0.4736
3	76.857	0.044	99.192	1.169	83.42	0.3823	99.804	0.576
4	76.647	0.524	99.652	0.362	82.98	0.4438	99.799	0.654
5	75.589	0.868	99.442	0.563	82.74	0.845	99.746	0.673

Figure S7 compare the desorption kinetics of the sorbent collected from the uptake kinetic experiments. From the first point of view, fast desorption was found with the high performance of the desorbing reagent (0.2 M HCl). Complete desorption was reached within 20 min, faster than the loading processes.

2.3. Treatment of Tannery Wastewater

Tannery effluents have a huge amount of chromium contaminants beside other associated elements with concentrations of 215.31, 0.334, 0.117, 0.488, and 0.513 mmol L⁻¹ of Cr(VI), Cd(II), Pb(II), Co(II), and Ni(II), respectively. The concentration of metal ions measured was close to 215.3 mmol Cr L⁻¹ and 0.17–0.52 mmol L⁻¹ for Ni(II), Cd(II), Co(II), and Pb(II). The large excess of chromate was calculated to be about 441.2 times for Co(II) and up to 1216.44, 644.64, and 419.8 times for Pb(II), Cd(II), and Ni(II), respectively. This concentration of chromate is too high to be consumed by the normal SD that is used in the synthetic solution (0.44 g L⁻¹). High S.D was used for the efficient removal of chromate (around 25–30 g L⁻¹). An evaluation of sorption properties was performed by comparing the removal efficiency of the grafted sorbent at L and UV with different SD (ranging from 1–30 g L⁻¹) at pH 4. The selectivity coefficients and the recovery efficiency are reported in Figure 5 and Figure S8 for both conditions of the grafted sorbent at different SD values. Figure S9 show a photo of the efficient removal of the chromium ions using MC-TDPD sorbent.

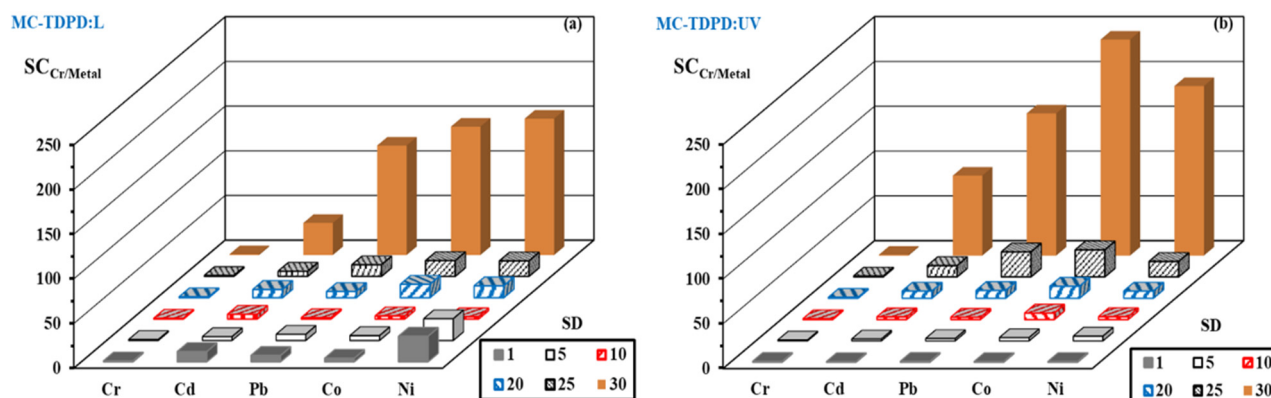


Figure 5. Selectivity coefficient of MC-TDPD at visible light (a) and Ultraviolet (b).

As expected, the high pH yields high removal of chromate, especially for the grafted sorbent in the UV emission. This is due to protonation of the sorbent at acidic pH, which facilitates repulsion with chromium ions (the source is sulfate, and it is presented as chromium cations).

The removal reached 99.57 and 97.5 for MC-TDPD:L and MC-TDPD:UV, respectively. In terms of the selectivity, it was found that the MC-TDPD:L is around (35–152), while this ratio increased using the UV condition to (89–242). The selectivity has the order:

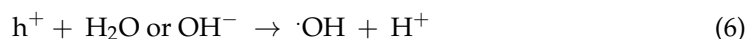
Cd(II) > Pb(II) > Co(II) > Ni(II) for both MC-TDPD:L and UV, while the recovery has order:

Cr(VI) > Cd(II) > Pb(II) > Ni(II) > Co(II) for MC-TDPD:UV, in which for MC-TDPD:L it become Cr(VI) > Cd(II) > Pb(II) > Ni(II) > Co(II).

As expected, the high S.D of the sorbent with this highly complex solution makes it difficult to reach the standard values for drinking water assessment but may fit the levels of irrigation and the livestock drinking water.

2.4. Effect of Light Mechanism on Cr(VI) Sorption

Functionalized chitosan (MC-TDPD) is characterized by the presence of the protonated amino, thion, and hydroxyl groups, while chitosan (MCH) has amino and hydroxyl groups; these groups act as active sites for metal ion binding [80]. Moreover, the magnetite nanoparticles (Fe₃O₄-NPs), considered the core material of both sorbents, are characterized by a small size that accelerates sorption kinetics and limit RIDE. In the presence of light-irradiation, the surface of Fe₃O₄ is excited due to photonic energy ($h\nu$) adsorption that is greater or equal to the bandgap of magnetite, leading to the liberation of electrons to form electron-lone pairs ($h^+ e^-$) (Equation (5)). The formed electron pairs are transferred to the magnetite surface to be involved in redox reactions. After that, the h^+ interacts with water (H₂O) or hydroxide ions (OH⁻) to form hydroxyl radicals ($\cdot\text{OH}$) and a high amount of H⁺ (Equation (6)). Finally, the replacement between Cr(VI) and H⁺ is enhanced.



3. Materials and Methods

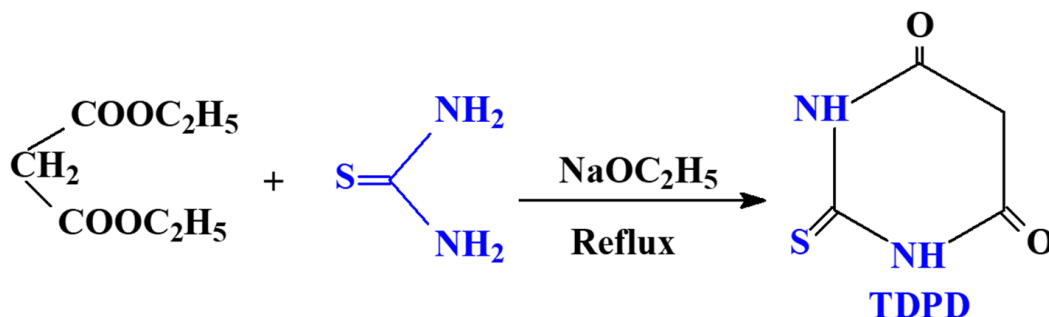
3.1. Materials

Chitosan with medium molecular weight (around 75–85% AD, acetylation degree), sodium hydroxide (NaOH: $\geq 97.0\%$), potassium persulfate (99.99%), thiourea (99%), sodium ethoxide solution (50%), Diethyl malonate (99%), and glutaraldehyde (25% in H₂O) were supplied from Merck company (Darmstadt-Germany). Ethanol (95%), epichlorohydrin ($\geq 99.9\%$), Ferrous sulfate (FeSO₄·7H₂O), and ammonium ferric sulfate ((NH₄)Fe(SO₄)₂·12H₂O) were supplied from Shanghai Macklin Biochemical Co., Ltd. (Shanghai, China). All other reagents are Prolabo products, which were used as received.

3.2. Sorbent Synthesis

3.2.1. Synthesis of 2-Thioxodihydropyrimidine-4,6(1H,5H)-Dione: TDPD

A mixture of thiourea (0.64 g; 10 mmol), sodium ethoxide solution (50%; 20 mL), and diethyl malonate (1.5 g, 10 mmol) were mixed in a reactor at room temperature. The reaction mixture was elevated to 70–80 °C for 10 h, then poured into an ice beaker in an acidic medium (0.1 M HCl solution). The mixture was left overnight for settling. The solid product was filtered off, dried, and then recrystallized using ethanol to obtain a white powder (yield 80%; mp above 300 °C); Scheme 2.



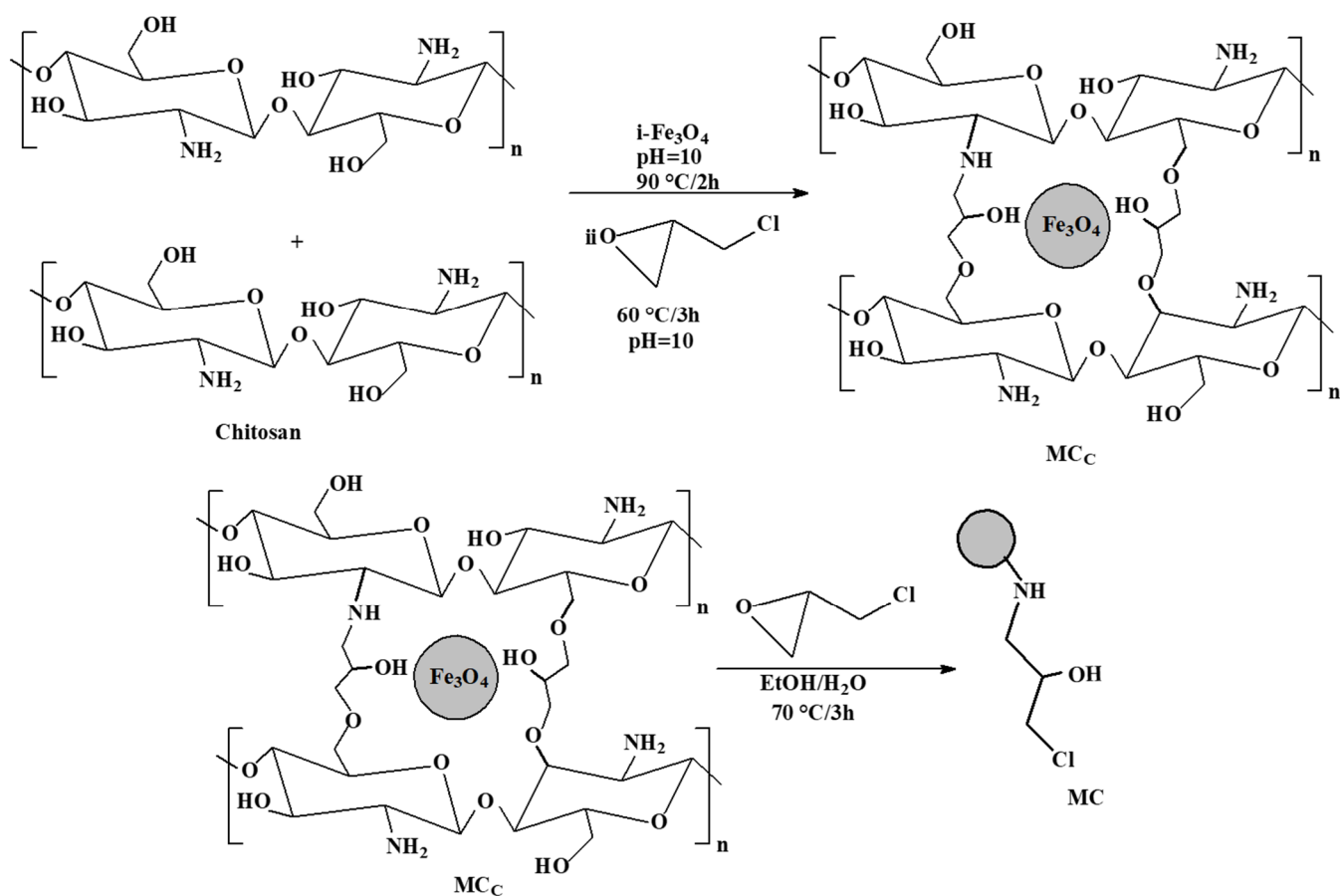
Scheme 2. Synthesis route of TDPD substrate.

3.2.2. Synthesis of Magnetite Nanoparticles

Magnetite nanoparticles were produced through thermal precipitation (called the Massart method, [81]). The mixture of ammonium ferric sulfate (7.35 g) and ferrous sulfate (5.0 g) was dissolved in distilled water. The temperature of the reaction was maintained at 50 °C for around 60 min with stirring. The pH of the solution was adjusted to 11 using 5–7 M NaOH solution for magnetite precipitation. The mixture was heated for 5 h at 50 °C. The produced precipitation was collected by magnetical separation, washed several times with water and ethanol, then dried at 50 °C for 20 h.

3.2.3. Synthesis of Activated Chitosan Nanoparticles

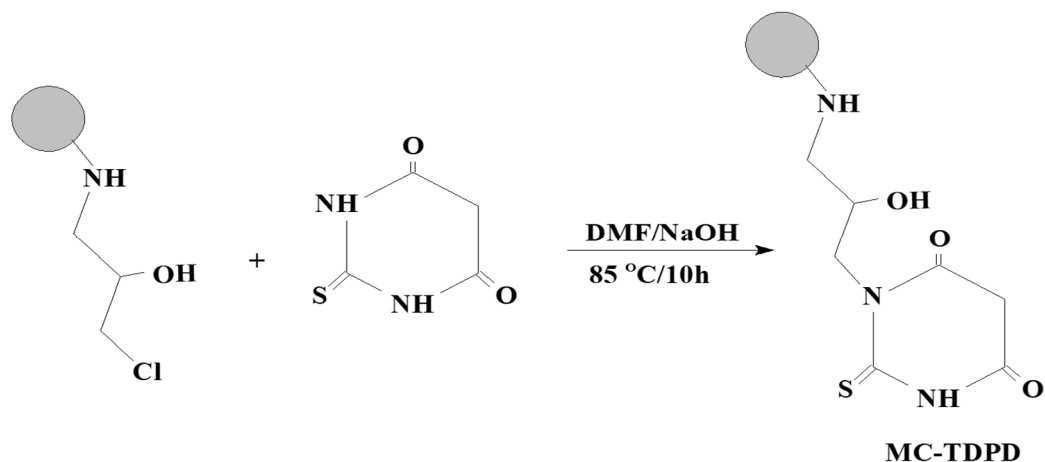
We dissolved 4 g of chitosan in 100 mL (7%, w/w) acetic acid solution, then added 4.0 g dried NPs, adjusting the pH of the solution to 10 using 5–7 M NaOH solution at 50 ± 5 °C. The reaction was maintained at 90 °C for 2 h. The formed precipitate underwent magnetical separation and was washed with distilled water. The stability of the sorbent was enhanced by a crosslinking process through the addition of epichlorohydrin (0.01 M EPI) in alkaline solution at pH 10 (adjusted by NaOH solution) for 3 h at 60 °C. The prepared precipitate (MCc) was separated magnetically, washed with water and acetone, and dried at 50 °C for 12 h. Further grafting of the crosslinked chitosan was performed by a reaction of EPI (18 mL) in ethanolic solution (1:1 ethanol/water) for activated crosslinked chitosan NPs. The reaction was refluxed for 3 h at 70 °C. The activated chitosan composite: MC (Scheme 3) was magnetically separated, washed with distilled water and acetone, and dried for 12 h at 50 °C.



Scheme 3. Synthesis of chitosan nanoparticles and activated chitosan (spacer arm).

3.2.4. Grafting of TDPD onto MC

The pH of the prepared TDPD solution (after the dissolution of 5 g in 100 mL DMF) was adjusted at pH 9.5–10 (using 5 M NaOH solution). Approximately 7 g of activated chitosan NPs were added to the solution at room temperature. The mixture underwent refluxed temperature (around 85–90 °C) for 10 h. The produced functionalized sorbent nanoparticles were magnetically separated, rinsed with water, and washed with ethanol before being air-dried at 50 °C for 10 h to produce MC-TDPD (9.8 g) Scheme 4.



Scheme 4. Synthesis of MC-TDPD sorbent.

3.3. Sorbent Characterization

FT-IR spectra were performed on dried samples before being mixed and ground with KBr using an IRTracer-100 FT-IR spectrometer, Shimadzu-Tokyo-Japan. The surface area and porosity were studied under nitrogen adsorption–desorption isotherms using Micromeritics, TriStar II-Norcross, GA, USA-system-77-K. The equation of the BET was used for adsorption. The samples were swept under nitrogen for 6 h at 130 °C. SEM analysis was performed using Phenom-ProX-SEM (Thermo Fisher Scientific, Eindhoven-Netherlands). The composition of the samples before and after metal-loading was semi-quantitatively characterized using EDX-analysis (energy dispersive X-ray analysis). A pH of zero charges (pH_{pzc}) was measured through the drift method [82]. The thermal decomposition, TGA analysis was performed using Netzsch STA, 449 F3 Jupiter, NETZSCH-Gerätebau-HGmbH, Selb-Germany. The analysis was achieved under a nitrogen atmosphere with a specification of $10\text{ }^{\circ}\text{C min}^{-1}$ (as a temperature ramp). The pH of the solution was adjusted using the compact pH ionometer; S220 Seven; Mettler-Toledo, Shanghai-China. Collected samples were firstly filtrated using 1.2- μm filter membranes before testing. The chromium element was measured before and after adsorption by ICPS-7510-Shimadzu, Tokyo-Japan. The photocatalytic activities were utilized using a 980 CW diode laser; Lambda Wave- Wrocław-Poland. The light power was about 0.84 W, and the size of the beam was approximately 8 mm^2 . On the other hand, the visible light was detected by the sunlight effect. The morphology and particle size of the composites were analyzed using transmission electron microscopy (TEM) (JEOL; 1010- JEOL Ltd.; Tokyo, Japan).

3.4. Sorption Studies

All experiments were investigated in visible light (sunlight) and under UV emission three times (triplicate experiments for verifying the reproducibility), and the average of the three experiments was plotted with the standard deviation. The sorption properties were investigated by the batch method under agitation velocity v : 210 rpm; a fixed mass of the sorbent (m , g) was used with a fixed volume amount of the Cr bearing solution (V , L). The sorption tests were investigated at around 23 °C (room temperature) with a sorbent dose of around 0.46 g L^{-1} . In the pH study, the initial (pH_{in}) values were varied between 1 to 6, which did not adjust during the sorption test, but the final pH was recorded (pH_{eq}) using a pH meter as specified in the above section. The contact time of the experiments (pH, kinetics, selectivity tests, sorption isotherms, etc.) was investigated in a fixed time of 24 h. In the sorption isotherms and kinetics, the pH_{in} was fixed at 4. The initial concentration (C_0 , mmol Cr L^{-1}) was varied for the sorption isotherms from 0.01 to $6.1\text{ mmol Cr L}^{-1}$. The loading capacity (q_{eq} , mmol g^{-1}) of the bound metal ions was determined from the mass balance equation: $q_{\text{eq}} = (C_0 - C_{\text{eq}}) \times V/m$, while the distribution ratio (D , L g^{-1}) was calculated through the following equation $D = q_{\text{eq}}/C_{\text{Equation}}$. The desorption kinetics were investigated for the loaded sorbent collected from the kinetic test using 0.2 M HCl solution. The used models for kinetics and isotherms were summarized with parameters in Table S2 and S3, respectively (see Supplementary Information).

3.5. Application on Tannery Effluent Solution

The wastewater was brought from the Robbiki Leather City on the 10th of Ramadan, Cairo-Egypt. The location was assigned at the GPS: N: $30^{\circ}17'89''$, E: $31^{\circ}76'840''$. Sorption was investigated in batch techniques at the pH 4.01 with different sorbent doses of $1\text{--}30\text{ g L}^{-1}$ for 24 h of contact time.

4. Conclusions

The high demand of water with limited resources requires inventing new methods with safe characteristics and cost-effective material; however, this is challenging. The synthesis of highly loaded sorbent for Cr(VI) ions based on crosslinked chitosan nanoparticles after grafting of heterocyclic moieties (MC-TDPD) for increasing the loading properties was the main target of this work. The sorbent showed promising sorption through application

on highly contaminated industrial tannery effluents. It was characterized by FTIR, TGA, BET (surface area), EA, SEM, and SEM-EDX analyses. The sorption was investigated using a batch method with high sorption capacity and fast kinetics compared with the non-grafted sorbent (MCH; as reference material). The sorption kinetics (30 and 25 for MC-TDPD in light and UV, respectively), were compared with 60 and 45 min for the non-functionalized material of MCH:L and MCH:UV, respectively. It was fitted using the PFORE and Langmuir and Sips for the sorption isotherms. The maximum sorption for the grafted sorbent was around 5.7 and 6.8 mmol Cr g⁻¹ at the L and UV, respectively, compared to 2.05 and 2.5 mmol Cr g⁻¹ for the crosslinked chitosan (without functionalization) in L and UV, respectively. This sorbent was tested for Cr recovery from the highly concentrated waste solution from tannery industries. The sorbent dose was varied for efficient sorption, and high sorption was reached for 25–30 gL⁻¹ in UV emission. This shows high performance and that it can be used as a promising tool for Cr(VI) removal

Supplementary Materials: The following supporting information can be downloaded at: <https://www.mdpi.com/article/10.3390/catal12070678/s1>, Figure S1: FTIR spectra of thiourea, TDPD, MC-TDPD, after sorption and after five cycles of sorption desorption; Figure S2: TGA and DrTG analyses of MC-TDPD sorbent T: 23–800 °C; Figure S3: pH_{zpc} of the MCH and MC-TDPD sorbents in range of pH 1–14; Figure S4: Cr(VI) species at pH 1–9; Figure S5: Cr(VI) uptake kinetics using MCH, MC-TDPD in light and UV condition- Modeling with the PSORE and RIDE; Figure S6: Cr(VI) sorption isotherms using MCH, MC-TDPD in light and UV condition- with the Freundlich equations; Figure S7: Desorption kinetics of MCH:L, MCH:UV, MC-TDPD:L and MC-TDPD:UV sorbents; Figure S8: Recovery efficient of MC-TDPD at visible light (a) and Ultraviolet (b); Figure S9: Removal efficient of Cr(VI) using MCH and MC-TDPD; Table S1: Elemental analysis of MCH and MC-TDPD sorbents; Table S2: Modeling of uptake kinetics [83–85]; Table S3: Modeling of sorption isotherms [86,87].

Author Contributions: Conceptualization, methodology M.H.Z., M.F.H., A.A.-H.A.-R., Y.W. and N.A.H.; software, Y.W., S.H.A. and H.H.A.; validation, G.E.-H., A.A.-H.A.-R. and H.I.M.; formal analysis, resources and investigation, M.H.Z., M.F.H., G.E.-H., A.A.-H.A.-R., Y.W., and H.I.M.; data curation, S.H.A., N.A.H. and H.H.A.; writing—original draft preparation, M.F.H. and N.A.H.; writing—review and editing, M.F.H. and N.A.H.; visualization, A.E.-S.G. and N.A.H.; supervision, M.F.H. and A.A.-H.A.-R.; project administration, S.H.A. and H.H.A.; funding acquisition, S.H.A. All authors have read and agreed to the published version of the manuscript.

Funding: Taif University for Researchers Supporting Project (TURSP-2020/83), Taif University, Saudi Arabia. Natural Science Foundation of China, National Natural Science Foundation of China [22066005, U1967218, 11975082] and NSFC 21976039.

Data Availability Statement: Data are available from the authors.

Acknowledgments: We acknowledge Taif University for the Researchers Supporting Project (TURSP-2020/83), Taif University, Saudi Arabia.

Conflicts of Interest: The authors declare no conflict of interest.

References

1. Fernández, P.M.; Viñarta, S.C.; Bernal, A.R.; Cruz, E.L.; Figueroa, L.I. Bioremediation strategies for chromium removal: Current research, scale-up approach and future perspectives. *Chemosphere* **2018**, *208*, 139–148. [CrossRef]
2. Cheriyan, D.; Choi, J.-H. A review of research on particulate matter pollution in the construction industry. *J. Clean. Prod.* **2020**, *254*, 120077. [CrossRef]
3. Zhang, H.; Li, C.; Chen, X.; Fu, H.; Chen, Y.; Ning, S.; Fujita, T.; Wei, Y.; Wang, X. Layered ammonium vanadate nanobelt as efficient adsorbents for removal of Sr²⁺ and Cs⁺ from contaminated water. *J. Colloid Interface Sci.* **2022**, *615*, 110–123. [CrossRef]
4. Wang, J.; Chen, C. Biosorption of heavy metals by *Saccharomyces cerevisiae*: A review. *Biotechnol. Adv.* **2006**, *24*, 427–451. [CrossRef]
5. Hamza, M.F. Uranium recovery from concentrated chloride solution produced from direct acid leaching of calcareous shale, Allouga ore materials, southwestern Sinai, Egypt. *J. Radioanal. Nucl. Chem.* **2018**, *315*, 613–626. [CrossRef]
6. Dogan, N.M.; Kantar, C.; Gulcan, S.; Dodge, C.J.; Yilmaz, B.C.; Mazmanci, M.A. Chromium (VI) bioremoval by *Pseudomonas* bacteria: Role of microbial exudates for natural attenuation and biotreatment of Cr (VI) contamination. *Environ. Sci. Technol.* **2011**, *45*, 2278–2285. [CrossRef]

7. Wang, Z.; Chen, G.; Wang, X.; Li, S.; Liu, Y.; Yang, G. Removal of hexavalent chromium by bentonite supported organosolv lignin-stabilized zero-valent iron nanoparticles from wastewater. *J. Clean. Prod.* **2020**, *267*, 122009. [[CrossRef](#)]
8. Liu, J.; Hao, D.; Sun, H.; Li, Y.; Han, J.; Fu, B.; Zhou, J. Integration of MIL-101-NH₂ into cellulosic foams for efficient Cr (VI) reduction under visible light. *Ind. Eng. Chem. Res.* **2021**, *60*, 12220–12227. [[CrossRef](#)]
9. Peng, H.; Guo, J. Removal of chromium from wastewater by membrane filtration, chemical precipitation, ion exchange, adsorption electrocoagulation, electrochemical reduction, electrodialysis, electrodeionization, photocatalysis and nanotechnology: A review. *Environ. Chem. Lett.* **2020**, *18*, 2055–2068. [[CrossRef](#)]
10. Godage, N.H.; Gionfriddo, E. Use of natural sorbents as alternative and green extractive materials: A critical review. *Anal. Chim. Acta* **2020**, *1125*, 187–200. [[CrossRef](#)]
11. Tripathi, D.K.; Ahmad, P.; Sharma, S.; Chauhan, D.K.; Dubey, N.K. *Nanomaterials in Plants, Algae, and Microorganisms: Concepts and Controversies: Volume 1*; Academic Press: Cambridge, MA, USA, 2017.
12. Fu, F.; Wang, Q. Removal of heavy metal ions from wastewaters: A review. *J. Environ. Manag.* **2011**, *92*, 407–418. [[CrossRef](#)]
13. Hamza, M.F.; Adel, A.-H.; Hawata, M.A.; El Araby, R.; Guibal, E.; Fouda, A.; Wei, Y.; Hamad, N.A. Functionalization of magnetic chitosan microparticles—Comparison of trione and trithione grafting for enhanced silver sorption and application to metal recovery from waste X-ray photographic films. *J. Environ. Chem. Eng.* **2022**, *10*, 107939. [[CrossRef](#)]
14. Wang, X.; Pehkonen, S.; Ray, A.K. Photocatalytic reduction of Hg (II) on two commercial TiO₂ catalysts. *Electrochim. Acta* **2004**, *49*, 1435–1444. [[CrossRef](#)]
15. Chenthamarakshan, C.; Rajeshwar, K. Photocatalytic reduction of divalent zinc and cadmium ions in aqueous TiO₂ suspensions: An interfacial induced adsorption–reduction pathway mediated by formate ions. *Electrochem. Commun.* **2000**, *2*, 527–530. [[CrossRef](#)]
16. Yeber, M.C.; Soto, C.; Riveros, R.; Navarrete, J.; Vidal, G. Optimization by factorial design of copper (II) and toxicity removal using a photocatalytic process with TiO₂ as semiconductor. *Chem. Eng. J.* **2009**, *152*, 14–19. [[CrossRef](#)]
17. Munusamy, S.; Sai Laxmi Aparna, R.; Gunneswara Subramanya Vara Prasad, R. Photocatalytic effect of TiO₂ and the effect of dopants on degradation of brilliant green. *Sustain. Chem. Processes* **2013**, *1*, 1–8.
18. Fouda, A.; Salem, S.S.; Wassel, A.R.; Hamza, M.F.; Shaheen, T.I. Optimization of green biosynthesized visible light active CuO/ZnO nano-photocatalysts for the degradation of organic methylene blue dye. *Heliyon* **2020**, *6*, e04896. [[CrossRef](#)]
19. Fouda, A.; Awad, M.A.; AL-Faifi, Z.E.; Gad, M.E.; Al-Khalaf, A.A.; Yahya, R.; Hamza, M.F. *Aspergillus flavus*-mediated green synthesis of silver nanoparticles and evaluation of their antibacterial, anti-candida, acaricides, and photocatalytic activities. *Catalysts* **2022**, *12*, 462. [[CrossRef](#)]
20. Hoffmann, M.; Martin, S.; Choi, W.; Bahnemann, D. Photocatalysis on TiO₂ surfaces—principles, mechanisms, and selected results. *Chem. Rev.* **1995**, *95*, 69–96. [[CrossRef](#)]
21. Zhang, L.; Qin, M.; Yu, W.; Zhang, Q.; Xie, H.; Sun, Z.; Shao, Q.; Guo, X.; Hao, L.; Zheng, Y. Heterostructured TiO₂/WO₃ nanocomposites for photocatalytic degradation of toluene under visible light. *J. Electrochem. Soc.* **2017**, *164*, H1086. [[CrossRef](#)]
22. Feng, X.; Shang, J.; Chen, J. Photoelectrocatalytic reduction of hexavalent chromium by Ti-doped hydroxyapatite thin film. *Mol. Catal.* **2017**, *427*, 11–17. [[CrossRef](#)]
23. Sane, P.; Chaudhari, S.; Nemade, P.; Sontakke, S. Photocatalytic reduction of chromium (VI) using combustion synthesized TiO₂. *J. Environ. Chem. Eng.* **2018**, *6*, 68–73. [[CrossRef](#)]
24. Alsharif, S.M.; Salem, S.S.; Abdel-Rahman, M.A.; Fouda, A.; Eid, A.M.; Hassan, S.E.-D.; Awad, M.A.; Mohamed, A.A. Multifunctional properties of spherical silver nanoparticles fabricated by different microbial taxa. *Heliyon* **2020**, *6*, e03943. [[CrossRef](#)]
25. Dai, X.; Nhung, N.T.H.; Hamza, M.F.; Guo, Y.; Chen, L.; He, C.; Ning, S.; Wei, Y.; Dodbiba, G.; Fujita, T. Selective adsorption and recovery of scandium from red mud leachate by using phosphoric acid pre-treated pitaya peel biochar. *Sep. Purif. Technol.* **2022**, *292*, 121043. [[CrossRef](#)]
26. Assadi, A.; Dehghani, M.H.; Rastkari, N.; Nasseri, S.; Mahvi, A.H. Photocatalytic reduction of hexavalent chromium in aqueous solutions with zinc oxide nanoparticles and hydrogen peroxide. *Environ. Prot. Eng.* **2012**, *38*, 5–16. [[CrossRef](#)]
27. Saied, E.; Eid, A.M.; Hassan, S.E.-D.; Salem, S.S.; Radwan, A.A.; Halawa, M.; Saleh, F.M.; Saad, A.H.; Saied, M.E.; Fouda, A. The catalytic activity of biosynthesized magnesium oxide nanoparticles (MgO-NPs) for inhibiting the growth of pathogenic microbes, tanning effluent treatment, and chromium ion removal. *Catalysts* **2021**, *11*, 821. [[CrossRef](#)]
28. Fouda, A.; Hassan, S.E.-D.; Saied, E.; Hamza, M.F. Photocatalytic degradation of real textile and tannery effluent using biosynthesized magnesium oxide nanoparticles (MgO-NPs), heavy metal adsorption, phytotoxicity, and antimicrobial activity. *J. Environ. Chem. Eng.* **2021**, *9*, 105346. [[CrossRef](#)]
29. Fouda, A.; Hassan, S.E.-D.; Saied, E.; Azab, M.S. An eco-friendly approach to textile and tannery wastewater treatment using maghemite nanoparticles (γ -Fe₂O₃-NPs) fabricated by *Penicillium expansum* strain (Kw). *J. Environ. Chem. Eng.* **2021**, *9*, 104693. [[CrossRef](#)]
30. Fouda, A.; Hassan, S.E.-D.; Abdel-Rahman, M.A.; Farag, M.M.; Shehal-Deen, A.; Mohamed, A.A.; Alsharif, S.M.; Saied, E.; Moghanim, S.A.; Azab, M.S. Catalytic degradation of wastewater from the textile and tannery industries by green synthesized hematite (α -Fe₂O₃) and magnesium oxide (MgO) nanoparticles. *Curr. Res. Biotechnol.* **2021**, *3*, 29–41. [[CrossRef](#)]
31. Cheng, Q.; Wang, C.; Doudrick, K.; Chan, C.K. Hexavalent chromium removal using metal oxide photocatalysts. *Appl. Catal. B Environ.* **2015**, *176*, 740–748. [[CrossRef](#)]
32. Wu, J.; Wang, J.; Du, Y.; Li, H.; Yang, Y.; Jia, X. Chemically controlled growth of porous CeO₂ nanotubes for Cr (VI) photoreduction. *Appl. Catal. B Environ.* **2015**, *174*, 435–444. [[CrossRef](#)]

33. Hamza, M.F.; Fouda, A.; Elwakeel, K.Z.; Wei, Y.; Guibal, E.; Hamad, N.A. Phosphorylation of guar gum/magnetite/chitosan nanocomposites for uranium (VI) sorption and antibacterial applications. *Molecules* **2021**, *26*, 1920. [[CrossRef](#)]
34. Colthup, N. *Introduction to Infrared and Raman Spectroscopy*; Elsevier: Amsterdam, The Netherlands, 2012.
35. Hamza, M.F.; Mahfouz, M.G.; Abdel-Rahman, A.A.-H. Adsorption of uranium (VI) ions on hydrazinyl amine and 1,3,4-thiadiazol-2 (3 H)-thion chelating resins. *J. Dispers. Sci. Technol.* **2012**, *33*, 1544–1551. [[CrossRef](#)]
36. Hamza, M.F.; Wei, Y.; Khalafalla, M.S.; Abed, N.S.; Fouda, A.; Elwakeel, K.Z.; Guibal, E.; Hamad, N.A. U (VI) and Th (IV) recovery using silica beads functionalized with urea-or thiourea-based polymers—Application to ore leachate. *Sci. Total Environ.* **2022**, *821*, 153184. [[CrossRef](#)]
37. Hamza, M.F.; Gamal, A.; Hussein, G.; Nagar, M.S.; Abdel-Rahman, A.A.H.; Wei, Y.; Guibal, E. Uranium (VI) and zirconium (IV) sorption on magnetic chitosan derivatives—effect of different functional groups on separation properties. *J. Chem. Technol. Biotechnol.* **2019**, *94*, 3866–3882. [[CrossRef](#)]
38. Hamza, M.F.; Roux, J.-C.; Guibal, E. Uranium and europium sorption on amidoxime-functionalized magnetic chitosan micro-particles. *Chem. Eng. J.* **2018**, *344*, 124–137. [[CrossRef](#)]
39. Hamza, M.F.; Wei, Y.; Mira, H.; Adel, A.-H.; Guibal, E. Synthesis and adsorption characteristics of grafted hydrazinyl amine magnetite-chitosan for Ni (II) and Pb (II) recovery. *Chem. Eng. J.* **2019**, *362*, 310–324. [[CrossRef](#)]
40. Hamza, M.F.; Mira, H.; Wei, Y.; Aboelenin, S.M.; Guibal, E.; Salem, W.M. Sulfonation of chitosan for enhanced sorption of Li (I) from acidic solutions—Application to metal recovery from waste Li-ion mobile battery. *Chem. Eng. J.* **2022**, *441*, 135941. [[CrossRef](#)]
41. Hamza, M.F.; Lu, S.; Salih, K.A.; Mira, H.; Dhmees, A.S.; Fujita, T.; Wei, Y.; Vincent, T.; Guibal, E. As (V) sorption from aqueous solutions using quaternized algal/polyethyleneimine composite beads. *Sci. Total Environ.* **2020**, *719*, 137396. [[CrossRef](#)]
42. Hamza, M.F.; Salih, K.A.M.; Abdel-Rahman, A.A.H.; Zayed, Y.E.; Wei, Y.; Liang, J.; Guibal, E. Sulfonic-functionalized algal/PEI beads for scandium, cerium and holmium sorption from aqueous solutions (synthetic and industrial samples). *Chem. Eng. J.* **2021**, *403*, 126399. [[CrossRef](#)]
43. Hamza, M.F.; Fouda, A.; Wei, Y.; El Aassy, I.E.; Alotaibi, S.H.; Guibal, E.; Mashaal, N.M. Functionalized biobased composite for metal decontamination—Insight on uranium and application to water samples collected from wells in mining areas (Sinai, Egypt). *Chem. Eng. J.* **2022**, *431*, 133967. [[CrossRef](#)]
44. Piasek, Z.; Urbanski, T. The infra-red absorption spectrum and structure of urea. *Bull. Acad. Pol. Sci.* **1962**, *X*, 113–120.
45. Hamza, M.F.; Salih, K.A.; Zhou, K.; Wei, Y.; Khoziem, H.A.A.; Alotaibi, S.H.; Guibal, E. Effect of bi-functionalization of algal/polyethyleneimine composite beads on the enhancement of tungstate sorption: Application to metal recovery from ore leachate. *Sep. Purif. Technol.* **2022**, *290*, 120893. [[CrossRef](#)]
46. Hamza, M.F.; Abdel-Rahman, A.A.-H. Extraction studies of some hazardous metal ions using magnetic peptide resins. *J. Dispers. Sci. Technol.* **2015**, *36*, 411–422. [[CrossRef](#)]
47. Lawrie, G.; Keen, I.; Drew, B.; Chandler-Temple, A.; Rintoul, L.; Fredericks, P.; Grondahl, L. Interactions between alginate and chitosan biopolymers characterized using FTIR and XPS. *Biomacromolecules* **2007**, *8*, 2533–2541. [[CrossRef](#)]
48. Coates, J. Interpretation of infrared spectra, a practical approach. In *Encyclopedia of Analytical Chemistry*; John Wiley & Sons, Ltd.: Hoboken, NJ, USA, 2006; pp. 1–23.
49. Yao, Z.; Zhang, C.; Ping, Q.; Yu, L.L. A series of novel chitosan derivatives: Synthesis, characterization and micellar solubilization of paclitaxel. *Carbohydr. Polym.* **2007**, *68*, 781–792. [[CrossRef](#)]
50. Wang, S.; Yu, D. Adsorption of Cd(II), Pb(II), and Ag(I) in aqueous solution on hollow chitosan microspheres. *J. Appl. Polym. Sci.* **2010**, *118*, 733–739. [[CrossRef](#)]
51. Tsai, H.S.; Wang, Y.Z.; Lin, J.J.; Lien, W.F. Preparation and properties of sulfopropyl chitosan derivatives with various sulfonation degree. *J. Appl. Polym. Sci.* **2010**, *116*, 1686–1693. [[CrossRef](#)]
52. Corazzari, I.; Nistico, R.; Turci, F.; Faga, M.G.; Franzoso, F.; Tabasso, S.; Magnacca, G. Advanced physico-chemical characterization of chitosan by means of TGA coupled on-line with FTIR and GCMS: Thermal degradation and water adsorption capacity. *Polym. Degrad. Stabil.* **2015**, *112*, 1–9. [[CrossRef](#)]
53. Chandra, S.; Saleem, H.; Sundaraganesan, N.; Sebastian, S. Experimental and theoretical vibrational spectroscopic and HOMO, LUMO studies of 1,3-dimethylbarbituric acid. *Ind. J. Chem.* **2009**, *48A*, 1219–1227.
54. Caetano, C.S.; Caiado, M.; Farinha, J.; Fonseca, I.M.; Ramos, A.M.; Vital, J.; Castanheiro, J.E. Esterification of free fatty acids over chitosan with sulfonic acid groups. *Chem. Eng. J.* **2013**, *230*, 567–572. [[CrossRef](#)]
55. Xiang, Y.; Yang, M.; Guo, Z.B.; Cui, Z. Alternatively chitosan sulfate blending membrane as methanol-blocking polymer electrolyte membrane for direct methanol fuel cell. *J. Membr. Sci.* **2009**, *337*, 318–323. [[CrossRef](#)]
56. Vieira, R.S.; Meneghetti, E.; Baroni, P.; Guibal, E.; Gonzalez de la Cruz, V.M.; Caballero, A.; Rodriguez-Castellon, E.; Beppu, M.M. Chromium removal on chitosan-based sorbents—An EXAFS/XANES investigation of mechanism. *Mater. Chem. Phys.* **2014**, *146*, 412–417. [[CrossRef](#)]
57. Hubbe, M.A.; Azizian, S.; Douven, S. Implications of apparent pseudo-second-order adsorption kinetics onto cellulosic materials: A review. *BioResources* **2019**, *14*, 7582–7626. [[CrossRef](#)]
58. Simonin, J.-P. On the comparison of pseudo-first order and pseudo-second order rate laws in the modeling of adsorption kinetics. *Chem. Eng. J.* **2016**, *300*, 254–263. [[CrossRef](#)]
59. Gao, B.; Li, Y.; Chen, Z. Adsorption behaviour of functional grafting particles based on polyethyleneimine for chromate anions. *Chem. Eng. J.* **2009**, *150*, 337–343. [[CrossRef](#)]

60. Henryk, K.; Jaroslaw, C.; Witold, Z. Peat and coconut fiber as biofilters for chromium adsorption from contaminated wastewaters. *Environ. Sci. Pollut. Res.* **2016**, *23*, 527–534. [[CrossRef](#)]
61. Li, Y.; Wei, Y.; Huang, S.; Liu, X.; Jin, Z.; Zhang, M.; Qu, J.; Jin, Y. Biosorption of Cr(VI) onto *Auricularia auricula* dreg biochar modified by cationic surfactant: Characteristics and mechanism. *J. Mol. Liq.* **2018**, *269*, 824–832. [[CrossRef](#)]
62. Tatarchuk, T.; Myslin, M.; Lapchuk, I.; Shyichuk, A.; Murthy, A.P.; Gargula, R.; Kurzydlo, P.; Bogacz, B.F.; Pedziwiatr, A.T. Magnesium-zinc ferrites as magnetic adsorbents for Cr(VI) and Ni(II) ions removal: Cation distribution and antistructure modeling. *Chemosphere* **2021**, *270*, 129414. [[CrossRef](#)]
63. Neagu, V.; Mikhalevsky, S. Removal of hexavalent chromium by new quaternized crosslinked poly(4-vinylpyridines). *J. Hazard. Mater.* **2010**, *183*, 533–540. [[CrossRef](#)]
64. Rawat, M.; Rawat, A.P.; Giri, K.; Rai, J.P.N. Cr(VI) sorption by free and immobilised chromate-reducing bacterial cells in PVA-alginate matrix: Equilibrium isotherms and kinetic studies. *Environ. Sci. Pollut. Res.* **2013**, *20*, 5198–5211. [[CrossRef](#)]
65. Neagu, V. Removal of Cr(VI) onto functionalized pyridine copolymer with amide groups. *J. Hazard. Mater.* **2009**, *171*, 410–416. [[CrossRef](#)]
66. Nasrollahpour, A.; Moradi, S.E. Hexavalent chromium removal from water by ionic liquid modified metal-organic frameworks adsorbent. *Microporous Mesoporous Mater.* **2017**, *243*, 47–55. [[CrossRef](#)]
67. Castro, L.; Blazquez, M.L.; Gonzalez, F.; Munoz, J.A.; Ballester, A. Heavy metal adsorption using biogenic iron compounds. *Hydrometallurgy* **2018**, *179*, 44–51. [[CrossRef](#)]
68. Yusof, A.M.; Malek, N.A.N.N. Removal of Cr(VI) and As(V) from aqueous solutions by HDTMA-modified zeolite Y. *J. Hazard. Mater.* **2009**, *162*, 1019–1024. [[CrossRef](#)]
69. Ajmal, M.; Demirci, S.; Uzun, Y.; Siddiq, M.; Aktas, N.; Sahiner, N. Introduction of double amidoxime group by double post surface modification on poly(vinylbenzyl chloride) beads for higher amounts of organic dyes, As(V) and Cr(VI) removal. *J. Colloid Interface Sci.* **2016**, *470*, 39–46. [[CrossRef](#)]
70. Arar, O. Preparation of anion-exchange cellulose for the removal of chromate. *J. Chil. Chem. Soc.* **2019**, *64*, 4471–4474. [[CrossRef](#)]
71. Ashraf, A.; Bibi, I.; Niazi, N.K.; Ok, Y.S.; Murtaza, G.; Shahid, M.; Kunhikrishnan, A.; Li, D.; Mahmood, T. Chromium(VI) sorption efficiency of acid-activated banana peel over organo-montmorillonite in aqueous solutions. *Int. J. Phytorem.* **2017**, *19*, 605–613. [[CrossRef](#)]
72. Hamza, M.F.; Hamad, D.M.; Hamad, N.A.; Adel, A.-H.; Fouda, A.; Wei, Y.; Guibal, E.; El-Etrawy, A.-A.S. Functionalization of magnetic chitosan microparticles for high-performance removal of chromate from aqueous solutions and tannery effluent. *Chem. Eng. J.* **2022**, *428*, 131775. [[CrossRef](#)]
73. Wang, Z.; Wang, Y.; Cao, S.; Liu, S.; Chen, Z.; Chen, J.; Chen, Y.; Fu, J. Fabrication of core@shell structural Fe-Fe₂O₃@PHCP nanochains with high saturation magnetization and abundant amino groups for hexavalent chromium adsorption and reduction. *J. Hazard. Mater.* **2020**, *384*, 121483. [[CrossRef](#)]
74. Aid, A.; Amokrane, S.; Nibou, D.; Mekatel, E.; Trari, M.; Hulea, V. Modeling biosorption of Cr(VI) onto *Ulva compressa* L. from aqueous solutions. *Water Sci. Technol.* **2018**, *77*, 60–69. [[CrossRef](#)]
75. Elwakeel, K.Z.; Elgarahy, A.M.; Guibal, E. A biogenic tunable sorbent produced from upcycling of aquatic biota-based materials functionalized with methylene blue dye for the removal of chromium(VI) ions. *J. Environ. Chem. Eng.* **2021**, *9*, 104767. [[CrossRef](#)]
76. Seliem, M.K.; Mobarak, M. Cr(VI) uptake by a new adsorbent of CTAB-modified carbonized coal: Experimental and advanced statistical physics studies. *J. Mol. Liq.* **2019**, *294*, 111676. [[CrossRef](#)]
77. Cui, B.; Chen, Z.; Wang, F.; Zhang, Z.; Dai, Y.; Guo, D.; Liang, W.; Liu, Y. Facile Synthesis of Magnetic Biochar Derived from Burley Tobacco Stems towards Enhanced Cr (VI) Removal: Performance and Mechanism. *Nanomaterials* **2022**, *12*, 678. [[CrossRef](#)] [[PubMed](#)]
78. Benettayeb, A.; Morsli, A.; Elwakeel, K.Z.; Hamza, M.F.; Guibal, E. Recovery of heavy metal ions using magnetic glycine-modified chitosan—application to aqueous solutions and tailing leachate. *Appl. Sci.* **2021**, *11*, 8377. [[CrossRef](#)]
79. Hamza, M.F.; Wei, Y.; Benettayeb, A.; Wang, X.; Guibal, E. Efficient removal of uranium, cadmium and mercury from aqueous solutions using grafted hydrazide-micro-magnetite chitosan derivative. *J. Mater. Sci.* **2020**, *55*, 4193–4212. [[CrossRef](#)]
80. Mohamed, A.E.; Elgammal, W.E.; Eid, A.M.; Dawaba, A.M.; Ibrahim, A.G.; Fouda, A.; Hassan, S.M. Synthesis and characterization of new functionalized chitosan and its antimicrobial and in-vitro release behavior from topical gel. *Int. J. Biol. Macromol.* **2022**, *207*, 242–253. [[CrossRef](#)]
81. Massart, R. Preparation of aqueous magnetic liquids in alkaline and acidic media. *IEEE Trans. Magn.* **1981**, *17*, 1247–1249. [[CrossRef](#)]
82. Lopez-Ramon, M.V.; Stoeckli, F.; Moreno-Castilla, C.; Carrasco-Marin, F. On the characterization of acidic and basic surface sites on carbons by various techniques. *Carbon* **1999**, *37*, 1215–1221. [[CrossRef](#)]
83. Crank, J. *The Mathematics of Diffusion*, 2nd ed.; Oxford University Press: Oxford, UK, 1975; p. 414.
84. Ho, Y.S.; McKay, G. Pseudo-second order model for sorption processes. *Process Biochem.* **1999**, *34*, 451–465. [[CrossRef](#)]
85. Zhang, R.; Leiviska, T. Surface modification of pine bark with quaternary ammonium groups and its use for vanadium removal. *Chem. Eng. J.* **2020**, *385*, 123967. [[CrossRef](#)]
86. Freundlich, H.M.F. Über die adsorption in lasungen. *Z. Phys. Chem.* **1906**, *57*, 385–470.
87. Tien, C. *Adsorption Calculations and Modeling*; Butterworth-Heinemann: Newton, MA, USA, 1994; p. 243.